RESEARCH ARTICLE

Vibrational Spectroscopic Studies (FT-IR, FT-Raman, UV) and Molecular Docking Analysis of Ebilfumin Drugs with Quantum Chemical Calculations

R. Solaichamy[1*], J. Karpagam[2], K. Govindarasu[2]

[1]*Department of Physics, SUN Arts and Science College, Thiruvannamalai-606 755, Tamil Nadu, India.*
[2]*Department of Physics, Annamalai University, Chidhambaram-608 002, Tamil Nadu, India.*

ABSTRACT: The solid phase FT-IR and FT-Raman spectra of Ebilfumin have been recorded in the regions 4000–400 cm^{-1} and 3500-50 cm^{-1} respectively. To interpret the experimental data, ab initio computations of the vibrational frequencies were carried out using the Gaussian 03 program followed by the full optimizations done using Density Functional Theory (DFT) at B3LYP/6-31G(d,p) level. The combined use of experiments and computations allowed a firm assignment of the majority of observed bands for the compound. The calculated stretching frequencies have been found to be in good agreement with the experimental frequencies. The electronic and charge transfer properties have been explained on the basis of Highest Occupied Molecular Orbitals (HOMOs), Lowest Unoccupied Molecular Orbitals (LUMOs). From the optimized geometry of the molecule, Molecular Electrostatic Potential (MEP) distributions of the title compound have been calculated in the ground state theoretically. The theoretical results showed good agreement with the experimental values. The molecular modelings are drawn and showed the bond length, bond angle, chemical reactivity, energy components (kcal/mol) and binding energy (kcal/mol) for all the title compounds and also protein for the ligand is shown. The study suggests further investigation on Ebilfumin for their biological activity importance.

KEYWORDS: Ebilfumin, FT-IR, FT-Raman, TED, NBO, Molecular Docking.

https://doi.org/10.29294/IJASE.5.1.2018.800-817

1. INTRODUCTION

Influenza presents a potential threat to human beings with seasonal epidemics and occasional severe pandemics, following reassortment of viral antigens. The World Health Organization estimates a total of 25 to 50 million cases each year resulting in 150,000 hospitalizations and 30,000 to 40,000 deaths in the United States alone, due to epidemic influenza. During pandemics the mortality and morbidity may be much higher, putting enormous pressure on basic health service provisions [1, 2].

Influenza illness is characterized by involvement of the lower respiratory tract (cough) accompanied with systemic complaints, including head ache, myalgia, and fever [3, 4]. Acute onset of cough and fever are good clinical predictors, associated with positive tests for influenza virus in 79% to 88% of patients during acute epidemics. Results depend to a large extent on detection and sampling methods as well as the severity of epidemic [5, 6]. Influenza viruses replicate predominantly in the airway epithelia, but also in various other host organs and tissues leading to airway congestion, inflammation, and necrosis [7]. Complications are frequent and severe complications include encephalitis, myelitis, myocarditis, intravascular coagulation and septic shock [8, 9]. Patients with under lying respiratory or cardiovascular disorders, children, older adults, and immunocompromised individuals display higher rates of severe illness and mortality [10]. Overall, acute respiratory tract infections severely influence morbidity and mortality during the winter and influenza plays a central role in this context [11, 12].

Neuraminidase inhibitors are recommended for the early treatment of influenza by the Centers for Disease Control and Prevention, the German Gesellschaft for Virologie, and the UK National Institute for Health and Care Excellence (NICE). The neuraminidase inhibitors Ebilfumin and Zanamivir have been demonstrated to reduce the duration and intensity of illness, but early intervention appears critical [13, 14]. Success of therapy depends on the sensitivity of causative viruses to these drugs. During the 2008–2009 winter seasons most seasonal H1N1 influenza subtypes had developed reduced sensitivity to Ebilfumin. In subsequent years this resistant virus type was a gain replaced by more sensitive's trains like H1N1 pdm 2009 or H3N2 [15].

Neuraminidase inhibitors are associated with adverse effects, including nausea, vomiting, psychiatric effects, and renal events. Safety issues, the importance of early administration, availability and the potential emergence of resistance compromise the broad applicability of neuraminidase inhibitors as recently highlighted by Jefferson et al [16]. The aim of the present work is characterized by Ebilfumin (ethyl (3R, 4R, 5S)-5-amino-4-acetamido-3-(pentan-3-yloxy)cyclohex-1-ene-1-

**Corresponding Author: solaichamy.r@gmail.com*

Received: 19.07.2018 **Accepted:** 18.08.2018 **Published on**: 24.08.2018

carboxylate). DFT method has a great accuracy in reproducing the experimental values in terms of geometry, dipole moment and vibrational frequency. The NBO analysis has also been carried out to elucidate information regarding the intra-molecular charge transfer within the molecule. The FT-IR, FT-Raman and UV-Visible spectra of the title molecule were carried out by using B3LYP/6-31G(d,p) level of calculation. The molecular docking is drawn and showed the bond length, bond angle, chemical reactivity, energy components (kcal/mol) and binding energy (kcal/mol) for all the title compounds and also protein for the ligand is shown.

2. EXPERIMENTAL DETAILS

The compound Oseltamaivir was purchased from Aldrich chemicals, USA and used as such to record the FT-IR and FT-Raman, UV spectra. The FT-IR spectrum of Oseltamaivir compound was recorded in the range of 4000–400 cm^{-1} on a BRUKER Optik GmbH FT-IR spectrometer using KBr pellet technique. The spectrum was recorded in the room temperature, with scanning speed of 10 cm^{-1}, and spectral resolution: 4 cm^{-1}. FT-Raman spectrum of the title compound was recorded using 1064 nm line of Nd:YAG laser as excitation wavelength in the region 3500–50 cm^{-1} on a BRUKER RFS 27: FT-Raman Spectrometer equipped with FT-Raman molecule accessory. The spectral resolution was set to 2 cm^{-1} in back scattering mode. The laser output was kept at 100mW for the solid sample. The ultraviolet absorption spectra of Ebilfumin were examined in the range 200–800 nm using Cary 500 UV–VIS–NIR spectrometer. The UV pattern is taken from a 10 to 5 M solution of Ebilfumin, dissolved in ethanol solvent. The theoretically predicted IR and Raman spectra at B3LYP/6-31G(d,p) level calculation along with experimental FT-IR and FT-Raman spectra are shown in **Figs. 2 and 3**.

3. COMPUTATIONAL DETAILS

The density functional theory DFT/B3LYP with the 6-31G(d,p) as basis set was adopted to calculate the properties of Oseltamaivir in the present work. All the calculations were performed using Gaussian 03W program package [17] with the default convergence criteria without any constraint on the geometry [18]. The assignments of the calculated wavenumbers are aided by the animation option of Gauss View 5.0 graphical interface for Gaussian programs, which gives a visual presentation of the shape of the vibrational modes along with available related molecules [19]. Furthermore, theoretical vibrational spectra of the title compound were interpreted by means of TED using the VEDA 4 program [20]. The optimized structural parameters were used in the vibrational frequency calculations at DFT levels to characterize all stationary points as minima. As the hybrid B3LYP functional tends to overestimate the fundamental normal modes of vibration, the computed frequencies were scaled with appropriate values to bring harmonization between the theoretical and experimental wavenumbers [21]. Vibrational frequencies were computed at DFT level which had reliable one-to-one correspondence with experimental IR and Raman frequencies [22]. The Natural Bond Orbital (NBO) calculations were performed using NBO 3.1 program [23] as implemented in the Gaussian 03W package at the DFT/B3LYP level; in order to understand various second order interactions between filled orbital of one subsystem and vacant orbital of another subsystem which is a measure of the intermolecular delocalization or hyper conjugation.

3.1. PREDICTION OF RAMAN INTENSITIES

The Raman activities (S_{Ra}) calculated with Gaussian 03W program converted to relative Raman intensities (I_{Ra}) using the following relationship derived from the intensity theory of Raman scattering [24]

$$I_i = \frac{f(\nu_o - \nu_i)^4 S_i}{\nu_i[1 - \exp(-hc\nu_i / kt)]}$$

Where, ν_0 is the laser exciting wavenumber in cm^{-1} (in this work, we have used the excitation wavenumber ν_0 = 9398.5 cm^{-1}, which corresponds to the wavelength of 1064 nm of an Nd-YAG laser), ν_i the vibrational wavenumber of the i^{th} normal mode (cm^{-1}) while S_i is the Raman scattering activity of the normal mode ν_i [25].

3.2. DOCKING STUDIES

The molecular structure of protein (PDB ID: 4M3M) was taken from RCSB Protein Data Bank [26]. Initial structures of Oseltamaivir were generated by ChemBioOffice 2008. The geometries of Oseltamaivir legand were subsequently optimized at DFT/B3LYP/ 6-31G (d,p) by Gaussian 03W. The molecular modeling docking calculations of Oseltamaivir legand with 4M3M protein were carried out by means of the Autodock tools (ADT) v1.5.4 [27] and Autodock 4.2.3 program from the Scripps Research Institute. In docking study, the search was extended over the whole receptor Oseltamaivir used as blind docking. The grid maps were generated with 0.375 Å spaces using a grid box of 70–70–70 Å. The search was carried out with the Lamarckian Genetic Algorithm because it has been pointed out to be most efficient, reliable and successful methods in Autodock [28]. The docking parameters used were as follows: GA population size = 150; maximum number of energy evaluation = 25, 00,000 and others used were default parameters. The docking conformation with the lowest binding free energy was used for further analysis by Molegro Molecular Viewer software [29].

4. RESULTS AND DISCUSSIONS

4.1. MOLECULAR GEOMETRY

The optimized geometry of Ebilfumin was shown in **Fig. 1** and the corresponding structural parameters of bond length and bond angle values were shown in Table 1. The optimized structural parameters of Ebilfumin were determined at the DFT/B3LYP and 6-31G(d,p) basis sets. From the theoretical values, it was found that some of the calculated parameters were slightly deviated from the experimental values, due to fact that the theoretical calculations belong to molecule in the gaseous phase and the experimental results belong to molecule in the solid state. The N-H bonds found to be shorter than the other bonds of Ebilfumin. The C-C bond length of the Cyclohexane ring varies from 1.343 Å-1.513 Å. Due to the O-H and NH_2 group substitution on the C3, C4 and $C5^{th}$

position of the cyclohexane ring, the C-C bond lengths are not same for example C1-C2=1.343 Å, C1-C6=1.513 Å, C2-C3=1.510 Å, C3-C4=1.543 Å, C4-C5=1.553 Å and C5-C6=1.539 Å calculated by B3LYP/DFT method. The C-O bond length on the Cyclohexane ring is 1.437 Å by DFT method. The C4-N19 and C5-N20 bond length is 1.461 Å and 1.468 Å calculated by DFT method. The C-H bond lengths of the Methylene (CH_2) group is C6-H27=1.099 Å and C6-H28=1.093 Å calculated by DFT method. The C-H bond lengths of Cyclohexane ring is C2-H23=1.087 Å, C3-H24=1.099 Å, C4-H25=1.092 Å and C5-H26=1.096 Å calculated by DFT method. The calculated double bond lengths C7-O8 were found as 1.216 Å by B3LYP method with 6-31G(d,p) basis sets, respectively.

As shown in Fig. 1, the molecular structure of the title compound contains one six-membered ring this ring (from C-1 to C-6) adopt chair conformations. The cyclohexane ring is disordered, with three of the C atoms distributed on two sites with approximately equal occupancy. In addition, one of the hydroxymethyl groups attached to C1 is disordered over the positions. The bond angle at point on the substitution is C2-C1-C6=123.3°calculated by DFT respectively. The unit –C7–O9–C21–C22- connected with C1 by the way of an equatorial bond, and the angles of N13-C5-H22 show 110.9° (DFT), C6-C1-C7 show 119.8° (DFT), C2-C1-C7 show 116.9° (DFT) and C1-C2-C3 show 123.8° (DFT), C1-C2-H23 show 118.1° (DFT) and C1-C6-C5 show 112.8° (DFT), C1-C6-H27 show 109.3° (DFT), C1-C6-H28 show 109.9° (DFT) and C1-C7-O8 show 125.2° (DFT), C1-C7-O9 show 111.7° (DFT) and O8-C7-O9 show 123.2° (DFT) like a bridge that aligned with the molecules.

Dihedral angles of cyclohexane part are found as C1-C2-C3-C4=14.39°, C2-C3-C4-C5=-43.13°, C3-C4-C5-C6=58.93°, C6- C1-C2-C3=-0.60° and C2-C1-C6-C5=16.14°. In case of twist form, the N-atom with the attached carbon 4 and 5 was considered are twisted about N19-C4-C5-C6=-64.10°, N19-C4-C5-N20=171.71° and N20-C5-C6-C1=82.69°, N20-C5-C6-H27=-154.72°, N20-C5-C6-H28=-39.25°. From **Table 1**, it is found that the bond lengths and bond angles calculated by B3LYP method with 6-31G (d,p) are consistent of the theoretical values. The deviations can be attributed to the fact that the theoretical calculations were aimed at the isolated molecules in the gaseous phase and the theoretical results were aimed at the molecule in the solid state. Despite these differences, the calculated geometrical parameters represent good approximation and they are the basis for the calculations of other parameters such as vibrational frequencies.

4.2. VIBRATIONAL ASSIGNMENTS

The vibrational spectral analysis is performed on the basis of characteristic vibrations of Carboxylic acid, Methylene and Cyclohexane ring vibrations. The observed and calculated frequencies using B3LYP/6-31G(d,p) basis set and along with their relative intensities, probable assignments and the Total Energy Distribution (TED) of the title molecule are summarized in **Table 2**. A complete assignment of the fundamentals was proposed based on the calculated TED values, infrared and Raman intensities. The title molecule consists of 50 atoms, which undergo 144 normal modes of vibrations, 48 modes of vibrations are stretching, 49 modes of vibrations are in-plane-bending and remaining 47 modes of vibrations are torsion. It agrees with C1 point group symmetry, all vibrations are active both in Raman and infrared absorption. The small difference between the experimental and calculated vibrational modes could be attributed to the fact that the experimental results belong to solid phase while the theoretical belong to isolated gaseous phase.

The calculated vibrational frequencies were scaled in order to improve the agreement with the experiment values. In our study we have followed scaling factor of 0.9608 for B3LYP/6-31G(d,p). After scaling with a scaling factor [30], the deviation from the experiments is less than 10 cm^{-1} with few exceptions. Comparison of the frequencies calculated at (B3LYP) method using 6-31G(d,p) basis set with experimental values reveals that the 6-31G(d,p) basis set result shows very good agreement with experimental observations, even for a complex molecular system. The vibrational assignments for different functional groups have been discussed below.

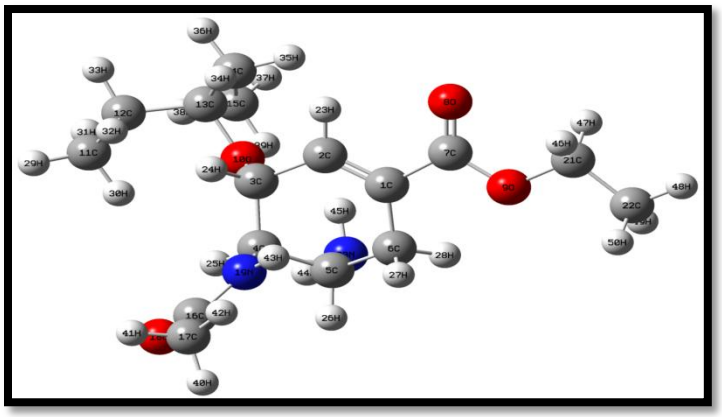

Fig.1. Optimized Molecular structure and atomic numbering of Ebilfumin

Table 1: Comparison of experimental and theoretical optimized parameter values of the Ebilfumin [bond length in (A°), angles in (◦)]

Bond length	B3LYP	Bond angle	B3LYP	Dihedral angle	B3LYP
C1-C2	1.343	C2-C1-C6	123.3	C6- C1-C2-C3	-0.60
C1-C6	1.513	C2-C1-C7	116.9	C6- C1-C2-H23	-178.85
C1-C7	1.498	C6-C1-C7	119.8	C7- C1-C2-C3	179.94
C2-C3	1.510	C1-C2-C3	123.8	C7- C1-C2-H23	1.69
C2-H23	1.087	C1-C2-H23	118.1	C2-C1-C6-C5	16.14
C3-C4	1.543	C3-C2-H23	118.2	C2-C1-C6-H27	-107.10
C3-O10	1.437	C2-C3-C4	112.2	C2-C1-C6-H28	137.26
C3-H24	1.099	C2-C3-O10	109.6	C7-C1-C6-C5	-164.42
C4-C5	1.553	C2-C3-H24	109.3	C7-C1-C6-H27	72.35
C4-N19	1.461	C4-C3-O10	108.8	C7-C1-C6-H28	-43.29
C4-H25	1.092	C4-C3-H24	107.5	C2-C1-C7-O8	-0.88
C5-C6	1.539	O10-C3-H24	109.3	C2-C1-C7-O9	178.69
C5-N20	1.468	C3-C4-C5	111.8	C6-C1-C7-O8	179.64
C5-H26	1.096	C3-C4-N19	109.5	C6-C1-C7-O9	-0.79
C6-H27	1.099	C3-C4-H25	108.5	C1-C2-C3-C4	14.39
C6-H28	1.093	C5-C4-N19	111.5	C1-C2-C3-O10	-106.61
C7-O8	1.216	C5-C4-H25	109.5	C1-C2-C3-H24	133.56
C7-O9	1.352	N19-C4-H25	105.7	H23-C2-C3-C4	-167.36
O9-C21	1.446	C4-C5-C6	110.3	H23-C2-C3-O10	71.65
O10-C13	1.442	C4-C5-N20	114.3	H23-C2-C3-H24	-48.18
C11-C12	1.532	C4-C5-H26	107.1	C2-C3-C4-C5	-43.13
C11-H29	1.095	C6-C5-N20	109.7	C2-C3-C4-N19	81.03
C11-H30	1.093	C6-C5-H26	108.1	C2-C3-C4-H25	-164.05
C11-H31	1.093	N20-C5-H26	107.0	O10-C3-C4-C5	78.35
C12-C13	1.541	C1-C6-C5	112.8	O10-C3-C4-N19	-157.50
C12-H32	1.098	C1-C6-H27	109.3	O10-C3-C4-H25	-42.58
C12-H33	1.098	C1-C6-H28	109.9	H24-C3-C4-C5	-163.34
C13-C14	1.539	C5-C6-H27	110.4	H24-C3-C4-N19	-39.19
C13-H34	1.101	C5-C6-H28	108.4	H24-C3-C4-H25	75.73
C14-C15	1.534	H27-C6-H28	105.8	C2-C3-O10-C13	-85.34
C14-H35	1.097	C1-C7-O8	125.2	C4-C3-O10-C13	151.66
C14-H36	1.098	C1-C7-O9	111.7	H24-C3-O10-C13	34.49
C15-H37	1.095	O8-C7-O9	123.2	C3-C4-C5-C6	58.93
C15-H38	1.092	C7-O9-C21	115.9	C3-C4-C5-N20	-65.26
C15-H39	1.093	C3-O10-C13	115.7	C3-C4-C5-H26	176.34
C16-C17	1.522	C12-C11-H29	110.3	N19-C4-C5-C6	-64.10
C16-O18	1.225	C12-C11-H30	110.8	N19-C4-C5-N20	171.71
C16-N19	1.371	C12-C11-H31	112.3	N19-C4-C5-H26	53.31
C17-H40	1.094	H29-C11-H30	107.8	H25-C4-C5-C6	179.28
C17-H41	1.093	H29-C11-H31	107.3	H25-C4-C5-N20	55.09
C17-H42	1.094	H30-C11-H31	108.1	H25-C4-C5-H26	-63.31
N19-H43	1.009	C11-C12-C13	117.1	C3-C4-N19-C16	130.97
N20-H44	1.018	C11-C12-H32	108.5	C3-C4-N19-H43	-52.76
N20-H45	1.018	C11-C12-H33	110.3	C5-C4-N19-C16	-104.70
C21-C22	1.516	C13-C12-H32	107.3	C5-C4-N19-H43	71.57
C21-H46	1.095	C13-C12-H33	107.7	H25-C4-N19-C16	14.24
C21-H47	1.094	H32-C12-H33	105.4	H25-C4-N19-H43	-169.50

Table 1: (Cont) Comparison of experimental and theoretical optimized parameter values of the Ebilfumin [Bond length in (A°), angles in (◦)]

Bond length	B3LYP	Bond angle	B3LYP	Dihedral angle	B3LYP
C22-H48	1.094	O10-C13-C12	110.9	C4-C5-C6-C1	-44.12
C22-H49	1.094	O10-C13-C14	107.6	C4-C5-C6-H27	78.47
C22-H50	1.094	O10-C13-H34	108.6	C4-C5-C6-H28	-166.06
		C12-C13-C14	117.2	N20-C5-C6-C1	82.69
		C12-C13-H34	106.2	N20-C5-C6-H27	-154.72
		C14-C13-H34	106.0	N20-C5-C6-H28	-39.25
		C13-C14-C15	117.4	H26-C5-C6-C1	-160.91
		C13-C14-H35	106.7	H26-C5-C6-H27	-38.32
		C13-C14-H36	107.9	H26-C5-C6-H28	77.15
		C15-C14-H35	108.1	C4-C5-N20-H44	-61.14
		C15-C14-H36	110.1	C4-C5-N20-H45	53.23
		H35-C14-H36	106.2	C6-C5-N20-H44	174.36
		C14-C15-H37	109.8	C6-C5-N20-H45	-71.27
		C14-C15-H38	112.8	H26-C5-N20-H44	57.29
		C14-C15-H39	110.9	H26-C5-N20-H45	171.66
		H37-C15-H38	107.4	C1-C7-O9-C21	179.85
		H37-C15-H39	107.8	O8-C7-O9-C21	-0.58
		H38-C15-H39	107.8	C7-O9-C21-C22	-178.99
		C17-C16-O18	121.8	C7-O9-C21-C22	59.30
		C17-C16-N19	115.4	C7-O9-C21-C22	-57.31
		O18-C16-N19	122.8	C3-O10-C13-C12	-84.72
		C16-C17-H40	108.7	C3-O10-C13-C14	145.93
		C16-C17-H41	108.6	C3-O10-C13-H34	31.63
		C16-C17-H42	114.0	H29-C11-C12-C13	167.51
		H40-C17-H41	107.3	H29-C11-C12-H32	46.03
		H40-C17-H42	108.9	H29-C11-C12-H33	-68.98
		H41-C17-H42	109.0	H30-C11-C12-C13	48.15
		C4-N19-C16	122.5	H30-C11-C12-H32	-73.32
		C4-N19-H43	118.5	H30-C11-C12-H33	171.67
		C16-N19-H43	118.9	H31-C11-C12-C13	-72.84
		C5-N20-H44	109.0	H31-C11-C12-H32	165.68
		C5-N20-H45	109.4	H31-C11-C12-H33	50.67
		H44-N20-H45	105.1	C11-C12-C13-O10	-57.24
		O9-C21-C22	107.5	C11-C12-C13-C14	66.79
		O9-C21-H46	108.7	C11-C12-C13-H34	-175.04
		O9-C21-H47	108.7	H32-C12-C13-O10	64.86
		C22-C21-H46	112.2	H32-C12-C13-C14	-171.11
		C22-C21-H47	112.2	H33-C12-C13-H34	-52.94
		H46-C21-H47	107.4	H33-C12-C13-O10	177.92
		C21-C22-H48	109.8	H33-C12-C13-C14	-58.06
		C21-C22-H49	111.0	H33-C12-C13-H34	60.12
		C21-C22-H50	111.0	O10-C13-C14-C15	50.34
		H48- C22-H49	108.3	O10-C13-C14-H35	-70.98
		H48-C22-H50	108.3	O10-C13-C14-H36	175.28
		H49-C22-H50	108.4	C12-C13-C14-C15	-75.37
				C12-C13-C14-H35	163.31
				C12-C13-C14-H36	49.57
				H34-C13-C14-C15	166.34
				H34-C13-C14-H35	45.02

Table 1: (Cont) Comparison of experimental and theoretical optimized parameter values of the Ebilfumin [Bond length in (A°), angles in (◦)]

Bond length	B3LYP	Bond angle	B3LYP	Dihedral angle	B3LYP
				H34-C13-C14-H36	-68.72
				C13-C14-C15-H37	-171.01
				C13-C14-C15-H38	69.17
				C13-C14-C15-H39	-51.94
				H35-C14-C15-H37	-50.42
				H35-C14-C15-H38	-170.25
				H35-C14-C15-H39	68.65
				H36-C14-C15-H37	65.17
				H36-C14-C15-H38	-54.66
				H36-C14-C15-H39	-175.76
				O18-C16-C17-H40	61.09
				O18-C16-C17-H41	-55.32
				O18-C16-C17-H42	-177.13
				N19-C16-C17-H40	-118.97
				N19-C16-C17-H41	124.62
				N19-C16-C17-H42	2.81.0
				C17-C16-N19-C4	178.33
				C17-C16-N19-H43	2.080
				O18-C16-N19-C4	-1.730
				O18-C16-N19-H43	-177.98
				O9-C21-C22-H48	-179.92
				O9-C21-C22-H49	60.37
				O9-C21-C22-H50	-60.18
				H46-C21-C22-H48	-60.41
				H46-C21-C22-H49	179.88
				H46-C21-C22-H50	59.33
				H47-C21-C22-H48	60.60
				H47-C21-C22-H49	-59.12
				H47-C21-C22-H50	-179.67

4.3.1. CYCLOHEXANE RING VIBRATIONS

The C-C stretching vibration of the Cyclohexane ring observed the FT-IR band at 1661 cm^{-1} and FT-Raman band at 1655 cm^{-1} and the computed scaled wavenumbers at 1642, 1184, 1110 and 890 cm^{-1} by DFT method. These modes are good agreement with literature [31, 32]. assigned C-C-C in-plane bending vibration at 882 and 578 cm^{-1} by DFT method. In our present work C-C-C in-plane bending vibration observed at 560 cm^{-1} in FT-IR spectrum and 553 cm^{-1} in FT-Raman spectrum predicted wave numbers are experimental method, which is good agreement with Cyclohexane derivatives.

The heteroaromatic structure shows the presence of C–H stretching vibration in the region 3100–3000 cm^{-1} which is the characteristics region for the ready identification of C–H stretching vibration [33]. In our present work C-H symmetric and anti symmetric stretching vibrations in ring CH_2 identified at 3064 cm^{-1} by DFT calculation. The ring CH_2 symmetric stretching vibration observed at 3059 cm^{-1} in FT-Raman spectrum. The 2995, 2945, 2915, 2898, 1642 and 1110 cm^{-1} by DFT method has been identified. The C–H in-plane bending frequencies occur in the region 1300–1000 cm^{-1}. In our present work C-C-C in-plane bending vibrations observed at 882, 578 and 248 cm^{-1} by DFT method and FT-Raman spectrum and the predicted wavenumbers at 553 and 246 cm^{-1} respectively. In our present work C-C-C in-plane bending vibrations observed at 560 cm^{-1} in FT-IR spectrum respectively. The out-of-plane bending vibrations are strongly coupled vibration and occur in the region 1000–750 cm^{-1} [34]. In our present work C-C-H out-of-plane bending vibrations observed at 1378 cm^{-1} in FT-IR spectrum and the predicted wavenumbers at 1379 cm^{-1} by DFT method respectively. Mode.nos 140 has been identified as C-C-C-C torsion vibration, which is good agreement with expected values.

4.3.2. AMINO GROUP VIBRATIONS

The amino groups are generally known as an electron donating group and the symmetric stretching vibrations of such groups usually lie in the range of 3450–3250 cm^{-1} [35]. The position of the absorption in this region depends upon the degree of hydrogen bonding and hence, upon the physical state of the sample or the polarity of the solvent. The free and interacting NH stretching vibrations of Cyclohexane cations give rise sharp peaks at higher and

lower wavenumbers [36]. In the present work, IR spectra at 3353 cm^{-1} arises due to the NH stretching of hydrogen bonded NH_2 group that interact with the acid residue by forming weak hydrogen bonds and symmetric stretching vibrations of these groups reveal the complex formation. The calculated values are presented in the range 3425–3350 cm^{-1} in B3LYP method with 6-31G(d,p) basis sets.

4.3.3. C-N VIBRATIONS

C-N bond lengths changes noticeably upon proton attachment to the Cyclohexane ring. The high frequency vibration for the Cyclohexane ring of melamine derivatives not involving in NH stretches is the in-phase stretch of the C-N bonds exogenous to the Cyclohexane ring. These C-N bonds involve the Cyclohexane ring carbon atom attached to the external nitrogen atom. This results in a weak Raman band in the range at 945 cm^{-1} indicating a high force constant for this bond, which is stiffened by resonance with the Cyclohexane ring bonds. The computed values of N-C stretching vibrations lie in the range at 1476, 1203, 1102, 1059 and 947 cm^{-1} by DFT method respectively. The shift in the ring modes results upon protonation which may be due to the sensitiveness of the ring modes to the orbital delocalization. It also causes increase in bond lengths of C4-N19 and C16-N19. This shows that the disruption of orbital delocalization takes place in the Cyclohexane ring which affects the character of the intra ring bonds which depends on the orbital delocalization. In our title molecules, the out-of-plane C-N-C bending vibrations have been observed at 336, 195 and 99 cm^{-1} by DFT method. The C-C-N- C computed value 85 cm^{-1} by DFT method respectively. The computed value of the ring stretching and bending modes very well agrees with the experimentally observed values.

4.3.4. C-O VIBRATIONS

The C-O stretching has been most extensively studied by infrared spectroscopy. The carboxyl group shows its main IR absorption bands of C-O around 1700–1780 cm^{-1} and C-O-C stretching vibrations are calculated by DFT method. The C-O stretching vibration band at 1724, 1712 cm^{-1} by DFT method and the corresponding IR and Raman vibration band C-O for 1720 cm^{-1} respectively. The computed values of C-O stretching vibrations are 1224, 1184, 1071, 1029, 899, 864, 851 and 824 cm^{-1} by DFT method. The band observed at 1211 and 868 cm^{-1} in the Raman spectrum is assigned to C-O stretching vibration mode respectively. The band observed at 1023/1029 cm^{-1} in the IR/Raman spectrum is assigned to C-O stretching vibration. The band observed at 141, 68 and 64 cm^{-1} spectrum is assigned to C-O-C torsion vibration by DFT method and Raman spectrum is assigned at 73 cm^{-1} respectively.

4.3.5. METHYLENE GROUP VIBRATIONS

For the assignments of CH_2 and CH_3 group frequencies, basically six fundamentals vibration can be associated to each CH_2 group namely, CH_2 symmetric stretch, antisymmetric stretch, scissoring and rocking modes, which belong to polarized in-plane vibrations . In addition to that, wagging and twisting mode of CH_2 group would be expected to be depolarized for out-of-plane bending vibration. The asymmetric CH_2 stretching vibration generally observed in the region 3000–2900 cm^{-1}, while the CH_2 symmetric stretch will appear between 2900 cm^{-1} and 2800 cm^{-1} [37]. In our present work the predicted wave numbers at 2985 cm^{-1} and 2937 cm^{-1} are identified as asymmetrical and symmetrical stretching vibrations respectively. For title molecule CH_2 anti symmetric and symmetric stretching vibrations observed at 2971 and 2936 cm^{-1} in FT-Raman and FT-IR spectrum respectively.

4.3.6. C–H VIBRATIONS

Aromatic compounds commonly exhibit multiple weak bands in the region 3100–3000 cm^{-1} due to aromatic C–H stretching vibration [38–41]. The bands appeared at 3059 cm^{-1} in FT-Raman spectrum are assigned to C–H ring stretching vibrations. The band identified at 3064 cm^{-1} in B3LYP methods are assigned to C–H ring stretching vibrations. The C–H in-plane and out-of-plane bending vibrations generally lie in the range of 1000–1300 cm^{-1} and 950–800 cm^{-1} [42, 43] respectively. In the present case, the C–H in plane bending vibrations of the compound is identified at 1251, 1247, 1241, 1147, 1138 and 1014 cm^{-1} in the B3LYP methods are assigned to C–H in-plane bending vibrations. The C–H in plane bending vibrations is observed at 1254/1274 cm^{-1} in FT-IR/FT-Raman spectrum. In our title molecules the C–H torsion vibrations is observed at 919 cm^{-1} by DFT method respectively.

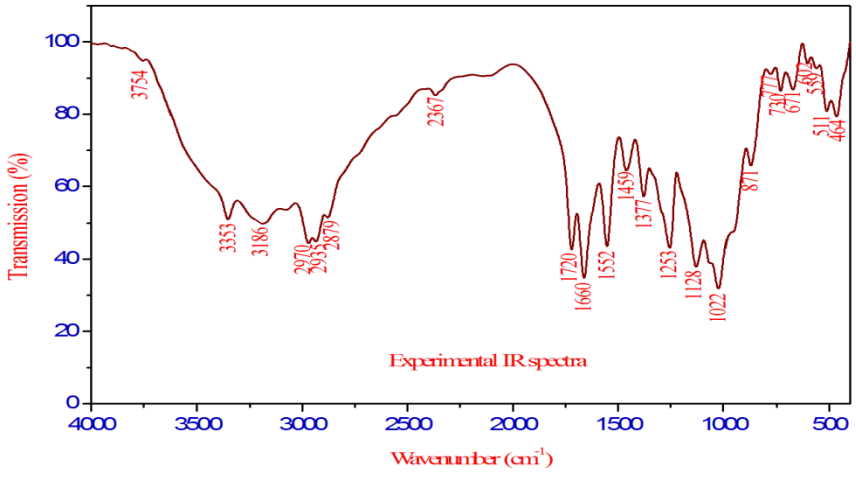

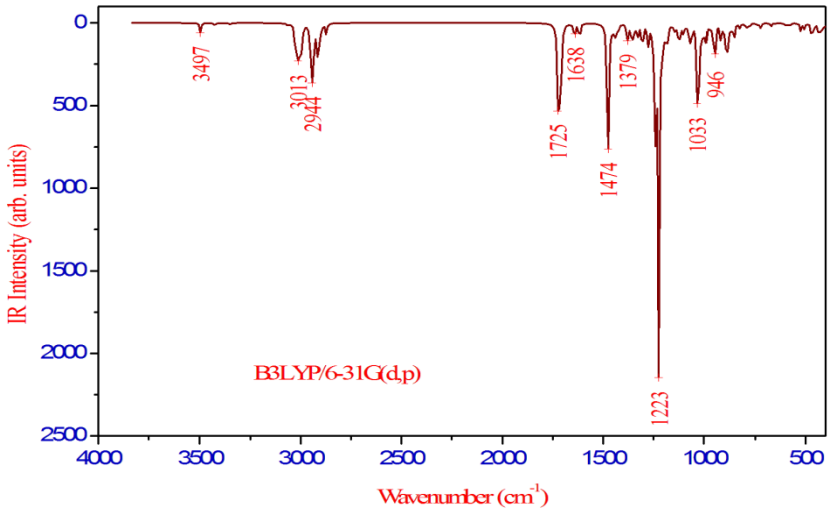

Fig.2. Comparison of experimental and theoretical B3LYP/6-31G (d,p) FT-IR spectrum for Ebilfumin

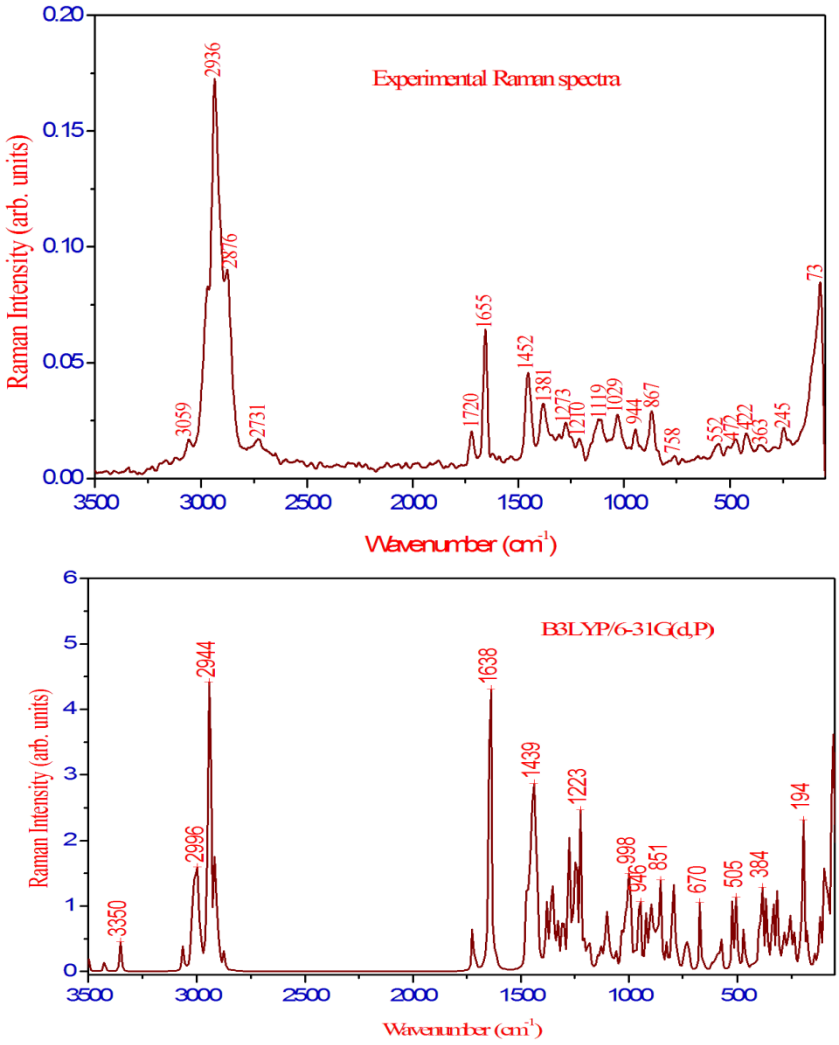

Fig.3. Comparison of experimental and theoretical B3LYP/6-31G (d,p) FT-Raman spectrum for Ebilfumin

Table 2. Comparison of the experimental and calculated vibrational spectra and proposed assignments of Ebilfumin

Mode No	Experimental wave numbers/cm^{-1}		Theoretical wave numbers/cm^{-1}				Vibrational assignments with TED (≥10%)
	FT-IR	FT-Raman	B3LYP/6-31G(d,p)				
			Unscaled	scaled	I_{IR}[a]	I_{Ra}[b]	
1			3640	3497	17.06	2.48	$\nu_{N19H43(100)}$
2			3565	3425	4.75	2.70	$\nu_{N20H44(100)}$
3	3353		3487	3350	1.85	5.75	$\nu_{N20H44(100)}$
4		3059	3189	3064	2.30	4.62	$\nu_{C2H23(99)}$
5			3150	3026	48.88	2.67	$\nu_{C11H30(79)}$
6			3143	3020	8.95	6.89	$\nu_{C17H40(95)}$
7			3140	3016	32.96	1.85	$\nu_{C22H49(82)}$
8			3138	3015	14.58	6.01	$\nu_{C17H40(98)}$
9			3137	3014	10.49	1.03	$\nu_{C11H30(77)}$
10			3132	3009	25.13	9.58	$\nu_{C22H48(94)}$
11			3127	3004	20.54	5.99	$\nu_{C11H29(87)}$
12			3122	2999	58.58	5.65	$\nu_{C4H25(93)}$
13			3121	2998	3.06	7.20	$\nu_{C11H29(83)}$
14			3117	2995	3.60	6.32	$\nu_{C6H28(92)}$
15	2971		3106	2985	7.14	7.19	$\nu_{C21H46(85)}$
16			3074	2953	30.78	10.13	$\nu_{C14H35(93)}$
17			3066	2946	16.02	9.65	$\nu_{C21H46(98)}$
18			3065	2945	38.77	10.43	$\nu_{C5H26(93)}$
19			3062	2942	31.23	23.12	$\nu_{C11H29(84)}$
20			3060	2940	29.61	8.28	$\nu_{C12H32(90)}$
21			3059	2939	8.87	12.19	$\nu_{C17H40(96)}$
22			3058	2938	13.82	4.56	$\nu_{C22H48(97)}$
23		2936	3057	2937	18.02	11.68	$\nu_{C11H29(86)}$
24			3039	2920	47.52	14.59	$\nu_{C14H35(80)}$
25			3034	2915	15.99	7.06	$\nu_{C6H27(91)}$
26			3029	2910	33.20	6.55	$\nu_{C12H32(74)}$
27			3017	2898	14.83	4.15	$\nu_{C3H24(88)}$
28			2991	2874	18.70	3.00	$\nu_{C13H34(92)}$
29	1720	1720	1794	1724	139.90	5.32	$\nu_{O8C7(84)}$
30			1782	1712	243.23	2.23	$\nu_{O18C16(83)}$
31	1661	1655	1709	1642	33.52	69.73	$\nu_{C2C1(69)}$
32			1682	1616	35.34	1.69	$\delta_{H45N20H44(71)}+\tau_{H44N20C5C4(24)}$
33			1537	1476	313.06	1.26	$\nu_{N19C16(22)}+\delta_{H43N19C16(49)}$
34			1532	1472	3.94	7.06	$\delta_{H29C11H31(66)}$
35			1531	1471	3.31	0.88	$\delta_{H46C21H47(64)}+\tau_{H46C21O9C7(18)}$
36	1460		1524	1464	3.77	5.84	$\delta_{H37C15H39(69)}$
37			1516	1456	6.30	4.14	$\delta_{H29C11H31(54)}$
38		1453	1512	1452	2.23	9.61	$\delta_{H46C21H47(75)}+\tau_{H49C22C21O9(15)}$
39			1507	1448	0.69	6.89	$\delta_{H29C11H30(63)}$
40			1502	1443	22.52	6.23	$\delta_{H48C22H49(75)}$
41			1501	1442	5.88	10.06	$\delta_{H40C17H41(66)}+\tau_{H40C17C16N19(22)}$
42			1499	1441	2.94	7.61	$\delta_{H32C12H33(78)}$
43			1488	1429	3.65	8.03	$\delta_{H32C12H33(67)}$
44			1485	1427	1.57	3.54	$\delta_{H27C6H28(75)}+\tau_{H42C17C16N19(10)}$
45			1484	1426	15.19	11.33	$\delta_{H27C6H28(72)}$

Table 2. (Cont) Comparison of the experimental and calculated vibrational spectra and proposed assignments of Ebilfumin

Mode No	Experimental wave numbers/cm^{-1}		Theoretical wave numbers/cm^{-1}				Vibrational assignments with TED (≥10%)
	FT-IR	FT-Raman	B3LYP/6-31G(d,p)				
			Unscaled	scaled	I_{IR}[a]	I_{Ra}[b]	
46			1439	1383	6.28	5.59	$\delta_{H48C22H49(72)}+\tau_{H46C21O9C7(12)}$
47		1381	1437	1381	11.92	1.88	$\delta_{H30C11H31(42)}$
48	1378		1436	1379	12.82	1.83	$\delta_{H26C5N20(21)}+\gamma_{C5C6C4H26(22)}$
49			1431	1375	8.53	2.78	$\delta_{H29C11H30(46)}+\tau_{H34C13O10C3(20)}$
50			1415	1360	13.53	5.29	$\delta_{H34C13O10(48)}$
51			1411	1355	23.16	6.06	$\delta_{H34C13O10(73)}$
52			1408	1352	3.31	1.75	$\delta_{H23C2C1(13)}$
53			1404	1349	1.46	2.97	$\tau_{H32C12C13C14(18)}$
54			1401	1346	7.80	1.24	$\tau_{H46C21O9C7(28)}$
55			1396	1341	2.39	0.44	$\delta_{H29C11H30(28)}+\tau_{H34C13O10C3(40)}$
56			1385	1331	13.26	4.11	$\tau_{H24C3O10C13(30)}$
57			1380	1326	14.81	2.88	$\delta_{H26C5N20(15)}+\tau_{H25C4N19C16(29)}+\gamma_{C5C6C4H26(12)}$
58			1361	1307	25.27	5.06	$\delta_{H24C3O10(24)}$
59			1355	1302	22.89	3.44	$\delta_{H24C3O10(28)}+\tau_{H32C12C13C14(10)}$
60			1332	1280	0.33	7.93	$\delta_{H23C2C1(36)}$
61		1274	1328	1276	37.87	11.89	$\delta_{H24C3O10(48)}$
62			1313	1261	3.96	5.98	$\delta_{H35C14C15(41)}$
63	1254		1302	1251	7.39	4.39	$\delta_{H32C12C13(27)}+\tau_{H33C12C13C14(15)}$
64			1298	1247	1.87	7.85	$\delta_{H46C21C22(78)}$
65			1292	1241	190.50	7.66	$\delta_{H27C6C1(24)}$
66		1211	1274	1224	631.63	17.59	$\nu_{O9C7(28)}$
67			1252	1203	46.65	3.84	$\nu_{N19C16(18)}+\delta_{H43N19C16(31)}$
68			1232	1184	56.89	5.51	$\nu_{C4C3(11)}+\gamma_{C5C6C4H26(12)}$
69			1194	1147	10.77	1.38	$\delta_{H27C6C1(37)}$
70			1185	1138	4.50	1.13	$\delta_{H46C21C22(16)}+\tau_{H46C21O9C7(58)}$
71	1129		1172	1126	16.06	2.35	$\nu_{C13C14(11)}+\tau_{H36C14C13C12(11)}$
72		1120	1167	1122	28.52	0.65	$\nu_{C13C14(12)}+\tau_{H30C11C12C13(18)}$
73			1155	1110	4.11	2.43	$\nu_{C5C6(12)}+\gamma_{N20C4C6C5(11)}$
74			1147	1102	11.86	3.61	$\nu_{N19C4(10)}$
75			1142	1097	8.14	5.13	$\nu_{C22C21(19)}+\delta_{C22C21O9(10)}+\tau_{H49C22C21O9(35)}$
76			1126	1082	1.91	2.03	$\tau_{H31C11C12C13(10)}$
77			1115	1071	53.85	1.01	$\nu_{O9C21(18)}$
78			1103	1059	12.34	1.77	$\nu_{N19C4(48)}$
79	1023	1029	1071	1029	268.44	7.37	$\nu_{O10C3(57)}$
80			1058	1016	8.28	3.24	$\nu_{C22C21(18)}$
81			1056	1014	8.91	0.94	$\delta_{H27C6H28(13)}+\tau_{H42C17C16N19(44)}+\gamma_{O18C17N19C16(14)}$
82			1049	1008	14.68	4.96	$\tau_{H35C14C13C12(14)}$
83			1037	997	15.02	10.02	$\nu_{C11C12(18)}$
84			1031	990	12.64	2.47	$\nu_{C13C14(21)}$
85			1030	989	14.13	2.31	$\nu_{C13C14(12)}+\delta_{H32C12C13(10)}$
86			1009	970	8.24	1.64	$\tau_{H40C17C16N19(31)}$
87			995	956	23.82	4.90	$\nu_{C17C16(10)}+\tau_{H40C17C16N19(12)}$
88		945	986	947	50.33	6.45	$\nu_{N19C16(12)}$
89			956	919	33.68	6.76	$\tau_{H23C2C1C6(35)}$
90			935	899	25.61	10.62	$\nu_{O10C13(23)}$

Table 2. (Cont) Comparison of the experimental and calculated vibrational spectra and proposed assignments of Ebilfumin

Mode No	Experimental wave numbers/cm^{-1}		Theoretical wave numbers/cm^{-1}				Vibrational assignments with TED (≥10%)
	FT-IR	FT-Raman	B3LYP/6-31G(d,p)				
			Unscaled	scaled	I_{IR}[a]	I_{Ra}[b]	
91			926	890	81.21	3.79	$\nu_{C5C6(15)}+\tau_{H44N20C5C4(23)}$
92			918	882	5.61	2.08	$\delta_{C1C2C3(11)}$
93	871		909	873	10.28	3.45	$\nu_{C13C14(51)}$
94		868	899	864	17.25	5.58	$\nu_{O9C21(17)}+\tau_{H49C22C21O9(10)}$
95			886	851	22.11	8.56	$\nu_{O9C21(15)}$
96			857	824	9.69	2.98	$\nu_{O9C7(12)}+\delta_{C22C21O9(18)}$
97			826	794	10.90	14.58	$\nu_{C11C12(11)}+\tau_{H35C14C13C12(12)}$
98			814	782	0.23	0.55	$\tau_{H46C21O9C7(77)}$
99	778		810	778	9.56	2.12	$\tau_{H35C14C13C12(13)}$
100		758	773	742	2.61	2.62	$\tau_{H33C12C13C14(31)}$
101	730		762	732	2.20	3.07	$\nu_{C12C13(22)}+\tau_{H35C14C13C12(25)}$
102			750	721	9.03	1.73	$\gamma_{O8C1O9C7(52)}$
103	672		696	669	5.37	6.97	$\gamma_{O8C1O9C7(12)}$
104			676	650	1.21	0.63	$\nu_{C12C13(11)}+\gamma_{O8C1O9C7(12)}$
105			638	613	0.97	1.52	$\tau_{H41C17C16N19(15)}+\gamma_{O18C17N19C16(47)}$
106	602		620	595	5.85	2.42	$\nu_{C17C16(15)}+\delta_{C17C16N19(11)}+\gamma_{O18C17N19C16(18)}$
107	560	553	601	578	5.83	4.71	$\delta_{C1C6C5(34)}$
108			543	522	13.75	6.46	$\delta_{C2C3O10(10)}$
109	511		524	504	11.81	7.78	$\delta_{C17C16O18(41)}$
110		473	490	470	14.85	3.69	$\delta_{O9C7C1(22)}$
111	464		478	459	20.94	1.50	$\delta_{C2C3O10(13)}+\tau_{H43N19C16C17(14)}$
112			449	432	31.02	0.81	$\delta_{C2C3O10(13)}+\tau_{H43N19C16C17(45)}$
113		423	433	416	16.10	0.66	$\tau_{H43N19C16C17(24)}$
114			413	397	10.21	7.23	$\tau_{H27C6C1C2(12)}$
115			401	385	0.46	6.86	$\tau_{H36C14C13C12(12)}$
116		364	380	365	8.33	8.47	$\delta_{C22C21O9(44)}$
117			350	336	5.02	9.82	$\delta_{C17C16N19(33)}$
118			328	316	3.76	6.72	$\delta_{C2C3O10(10)}$
119			316	304	7.10	1.28	$\delta_{C2C3O10(19)}$
120			302	290	16.16	1.70	$\delta_{C11C12C13(12)}$
121			289	278	0.18	4.61	$\tau_{H29C11C12C13(10)}+\gamma_{C14C12O10C13(15)}$
122			269	259	17.93	5.42	$\tau_{H44N20C5C4(45)}$
123			262	252	8.17	2.86	$\tau_{H50C22C21O9(50)}$
124		246	258	248	5.24	0.45	$\delta_{C7C1C2(17)}$
125			246	237	1.65	2.87	$\delta_{C11C12C13(13)}+\gamma_{C14C12O10C13(14)}$
126			218	209	1.71	1.50	$\delta_{C13O10C3(10)}$
127			210	201	2.29	2.05	$\tau_{H29C11C12C13(24)}$
128			203	195	3.36	12.81	$\delta_{C4N19C16(37)}$
129			182	175	0.38	3.50	$\delta_{C13C14C15(28)}+\tau_{H39C15C14C13(13)}$
130			146	141	0.68	1.38	$\tau_{C21O9C7C1(35)}$
131			124	119	0.69	3.07	$\tau_{C11C12C13O10(14)}$
132			121	116	1.48	2.10	$\delta_{C13O10C3(12)}+\tau_{C11C12C13O10(17)}$
133			103	99	2.37	6.91	$\delta_{C4N19C16(11)}+\tau_{C21O9C7C1(14)}+\gamma_{N19C3C5C4(16)}$
134			96	93	0.09	3.29	$\delta_{O9C7C1(20)}+\tau_{C17C16N19C4(13)}$
135			89	85	1.95	8.44	$\tau_{C17C16N19C4(24)}$
136		73	71	68	0.80	3.94	$\tau_{C7O9C21C22(18)}$

Table 2. (Cont) Comparison of the experimental and calculated vibrational spectra and proposed assignments of Ebilfumin

Mode No	Experimental wave numbers/cm^{-1}		Theoretical wave numbers/cm^{-1}				Vibrational assignments with TED (≥10%)
	FT-IR	FT-Raman	B3LYP/6-31G(d,p)				
			Unscaled	scaled	I_{IR}[a]	I_{Ra}[b]	
137			67	64	0.37	8.72	$\tau_{C7O9C21C22(38)}$
138			57	54	4.04	14.67	$\tau_{C17C16N19C4(34)}$
139			54	52	0.25	7.15	$\tau_{C12C13C14C15(50)}$
140			37	35	1.96	27.35	$\tau_{C4C3C2C1(15)}$
141			33	32	2.64	3.84	$\tau_{C4C3O10C13(62)}$
142			28	27	0.27	5.26	$\tau_{C3O10C13C12(48)}$
143			22	21	0.46	38.89	$\tau_{C3O10C13C12(53)}+\gamma_{C7C2C6C1(28)}$
144			17	16	3.30	100.00	$\tau_{C3C4N19C16(17)}$

ν-stretching; δ-in-plane-bending; γ-out-of-plane bending; τ-torsion; w-weak; s-strong; vs-very strong; vw-very weak; m-medium.
[a]I_{IR}-IR Intensity (Kmmol^{-1});
[b]I_{Ra}-Raman intensity (Arb units) (intensity normalized to 100%)

Table 3. Second order Perturbation theory analysis of Fock Matrix in NBO basis for Ebilfumin.

Donor (i)	E_D (i)(e)	Acceptor(j)	E_D (j)(e)	E(2)[a] KJ mol^{-1}	E(j)-E(i)[b] a.u	F(i,j)[c] a.u
π(C1-C2)	1.880	π*(C7-O8)	0.264	18.90	0.29	0.068
LP(1)O8	1.976	RY*(1)C7	0.021	15.03	1.53	0.135
LP(2)O8	1.844	σ*(C1-C7)	0.069	18.57	0.68	0.102
LP(2)O8	1.844	σ*(C7-O9)	0.099	33.42	0.63	0.132
LP(2)O9	1.786	π*(C7-O8)	0.264	49.01	0.33	0.115
LP(2)O18	1.976	RY*(1)C16	0.017	15.97	1.45	0.136
LP(2)O18	1.858	σ*(C16-C17)	0.056	20.70	0.61	0.103
LP(2)O18	1.858	σ*(C16-N19)	0.078	25.70	0.71	0.122
LP(1)N19	1.713	π*(C16-O18)	0.289	64.62	0.28	0.120
π*(C7-O8)	0.264	π*(C1-C2)	0.074	30.99	0.04	0.073

E_D -means Electron Density
[a]E(2)- means energy of hyper conjugative interactions
[b]Energy difference between donor and acceptor i and j NBO orbitals
[c]F(i,j) is the Fock matrix element between i and j NBO orbitals

4.3. NBO ANALYSIS

In the NBO analysis, the electron wave functions are interpreted in terms of a set of occupied Lewis type (bond or lone pair) and a set of unoccupied non-Lewis (anti-bond or Rydberg) localized NBO orbitals. The delocalization of Electron Density (ED) between these orbitals corresponds to a stabilizing donor acceptor interaction. A useful aspect of the NBO method is that it gives information about interactions in both filled and virtual orbital spaces, which could enhance the analysis of intra- and intermolecular interactions.

The second-order Fock matrix was carried out to evaluate the donor acceptor interactions in the NBO basis. The interactions result in a loss of occupancy from the localized NBO of the idealized Lewis structure into an empty nonLewis orbital. For each donor (i) and acceptor (j), the stabilization energy $E_{(2)}$ associated with the delocalization i / j is estimated as

$$E_2 = \Delta E_{ij} = q_i \frac{F(i,j)^2}{\varepsilon_j - \varepsilon_i}$$

where q_i is the donor orbital occupancy, ε_i and ε_j are diagonal elements and F(i, j) is the off-diagonal NBO Fock matrix element.

The molecular interaction is formed by the orbital overlap between π(C1-C2) → π*(C7-O8), π*(C7-O8) → π(C1-C2) resulting intra molecular charge transfer with stabilization energy is about 18.90, and 30.99 kCal/mol. As can be seen from this **Table 3**, NBO analysis revealed that the intramolecular interaction is formed by the orbital overlap between LP(1)N19 → π*(C16-O18) bond orbital, which results intramolecular charge transfer causing stabilization energy 64.62 kCal/mol of the system. The energy contribution of LP(2)O8 → σ*(C1-C7), σ*(C7-O9), LP(2)O18 → σ*(C16-C17), σ*(C16-N19) are 18.57, 33.42, 20.70 and 25.70 kCal/mol, respectively.

4. 5. ELECTRONIC PROPERTIES

4.5.1. UV-VISIBLE SPECTRAL ANALYSIS

The highest occupied molecular orbitals (HOMOs) and the lowest-lying unoccupied molecular orbitals (LUMOs) are named as frontier molecular orbitals (FMOs). The FMOs play an important role in the optical and electric properties, as well as in quantum chemistry and UV-VIS spectra [44]. Absorption maxima (λ_{max}) (nm) for lower-lying singlet states of the molecule of the molecule have been calculated by TD-DFT/B3LYP method. The computed properties such as absorption wavelength (λ), excitation energies (E), frontier molecular orbital energies, and oscillator strengths (f) are listed in **Table 4**. **Fig. 4** shows the observed UV-Vis spectra of title compound in ethanol solvent. For TD-DFT calculations, the theoretical absorption band was predicted at 252.57 nm with oscillator strength being 0.0023 in ethanol solvent and at 258.66 nm with oscillating strength 0.0115 in gas phase can easily be seen that this corresponds to the experimental absorption at 235 nm.

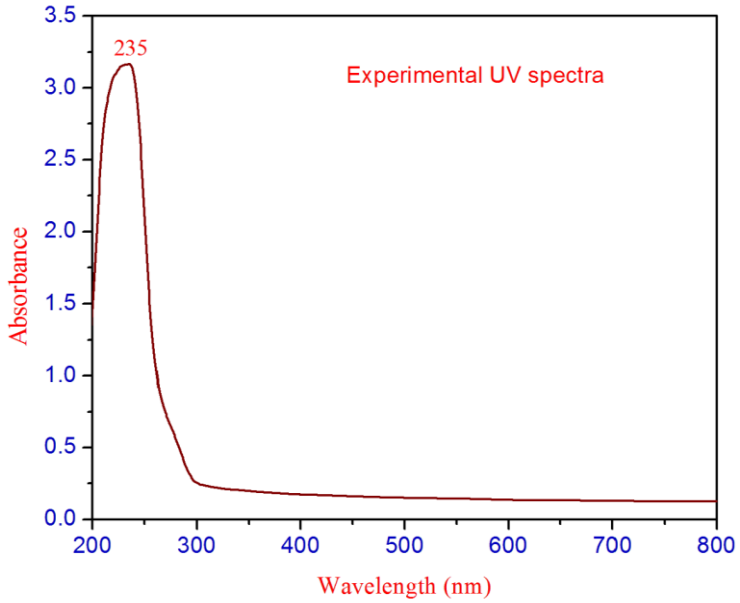

Fig.4. UV-Visible spectrum (Ethanol) of Ebilfumin

Table 4. The experimental and computed absorption wavelength λ (nm), excitation energies E (eV), absorbance and oscillator strengths (*f*) of Ebilfumin in Ethanol solution and gas phase.

Experimental		TD-DFT/B3LYP/6-31G(d,p)					
Ethanol		Ethanol			Gas		
λ(nm)	Abs.	λ(nm)	E(eV)	f(a.u)	λ(nm)	E(eV)	f(a.u)
		299.79	4.1357	0.0068	307.79	4.0281	0.0036
		265.37	4.6721	0.0277	265.33	4.6728	0.0084
235	3.1664	252.57	4.9089	0.0023	258.66	4.7933	0.0115

4.5.2. HOMO-LUMO Analysis

Molecular orbitals, when viewed in a qualitative graphical representation, it can provide insight into the nature of reactivity, and some of the structural and physical properties of molecules. Both the highest occupied molecular orbital (HOMO) and lowest unoccupied molecular orbital (LUMO) are the main orbitals taking part in chemical reactions. The HOMO energy characterizes the ability of electron donating; LUMO characterizes the ability of electron accepting and the gap between HOMO and LUMO characterize the molecular chemical stability. Energy difference between HOMO and LUMO orbital is called as energy gap that is an important stability for structures [45]. The energy gap is largely responsible for the chemical and spectroscopic properties of the molecules. This also used by the frontier electron density for predicting the most reactive position in p-electron systems and also explains several types of reactions in conjugated systems [46]. The title molecule is given in **Fig. 5**. In addition, according to B3LYP/6-31G(d,p) calculation, the energy band gap of the title molecule is - 4.6423 eV. The positive and negative phase is represented in red and green color, respectively.

HOMO energy = -5.9509 eV
LUMO energy = -1.3086 eV
HOMO-LUMO energy gap = - 4.6423 eV.

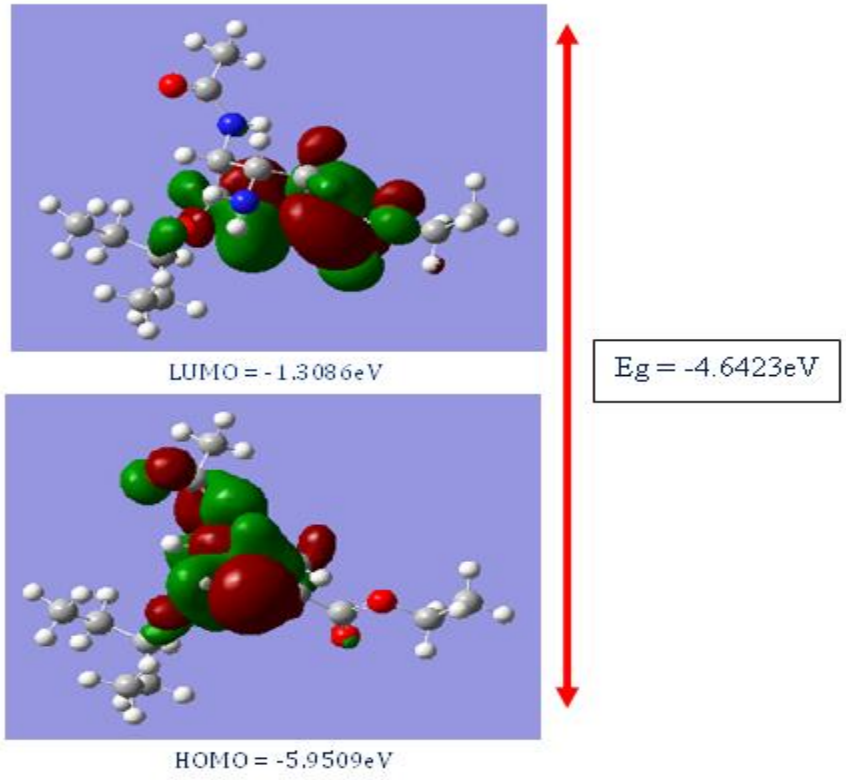

Fig.5. The atomic orbital compositions of the frontier molecular orbital for Ebilfumin

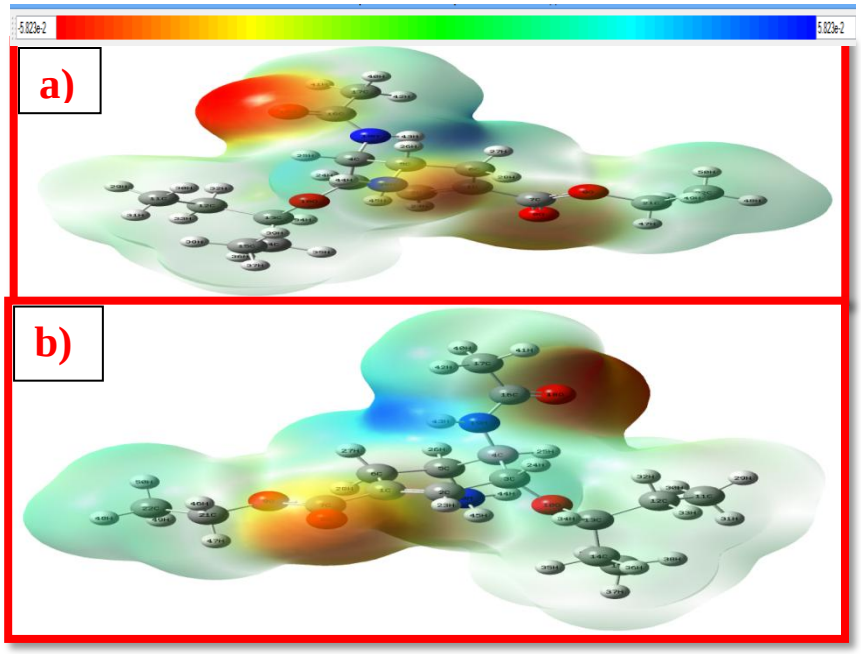

Fig.6. a) Front view b) back view of Molecular electrostatic Potential map (MEP) for Ebilfumin

4.5.3. MOLECULAR ELECTROSTATIC POTENTIAL (MEP) ANALYSIS

In order to grasp the molecular interactions, the Molecular Electrostatic Potentials (MEPs) are used. Recently, the MEPs have been used for interpreting and predicting relative reactivities sites for eletrophilic and nucleophilic attack, investigation of biological recognition, hydrogen bonding interactions, studies of molecular cluster, crystal behavior, correlation and prediction of a wide range of macroscopic properties [47]. The MEP diagram (front and back view) of the Ebilfumin molecule is shown in **Fig. 6**, in color quantity from -5.823 e-2 (deepest red) to be able to +5.823 e-2 (deepest blue). The color scheme for the MEP surface will be partially negative charge or maybe red-electron rich; partially positive charge or maybe blue-electron deficient; yellow slightly electron packed region; light blue-slightly electron deficient region, For the title molecule yellow color represents the electron packed region which is mostly cover the oxygen atoms and also the positive region is actually over the NH group. Green color represents the zero potential regions mostly over the all protons.

4.5.4. MOLECULAR MODELING ANALYSIS

Molecular docking studies were performed to investigate the binding affinities of the newly compound Ebilfumin and the human Influenza protein [4M3M]. The title molecule is given in **Fig. 7** and the values are tabulated in Table 5. The ligand-protein complex stability was successfully made by some features such as hydrogen bond interactions, Vander Waals forces, π→π stacking interactions, hydrophobic interactions. These interactions between the drug and receptor depend upon the nature of functional groups present in the ligand. On ligand preparation (by ligprep module) of compound Ebilfumin structures were obtained. Water molecules and co-crystallized ligands were removed. Molecular docking studies were performed to investigate the higher binding affinities and total intermol energy of the newly compound Ebilfumin is -4.97 kcal/ mol and -1.81 kcal/ mol lower binding affinities and total intermol energy of the title molecules is -8.00 kcal/ mol and -5.00 kcal/ mol respectively.

Table. 5 Comparison of Est. Free Energy of Binding, Total Intermol. Energy of Ebilfumin

Mode	Est. Free Energy of Binding	Total Intermol. Energy
1	-4.97 kcal/ mol	-8.00 kcal/ mol
2	-3.26 kcal/ mol	-6.91 kcal/ mol
3	-2.53 kcal/ mol	-6.13 kcal/ mol
4	-2.46 kcal/ mol	-5.61 kcal/ mol
5	-2.26 kcal/ mol	-5.40 kcal/ mol
6	-1.96 kcal/ mol	-5.34 kcal/ mol
7	-1.81 kcal/ mol	-5.00 kcal/ mol

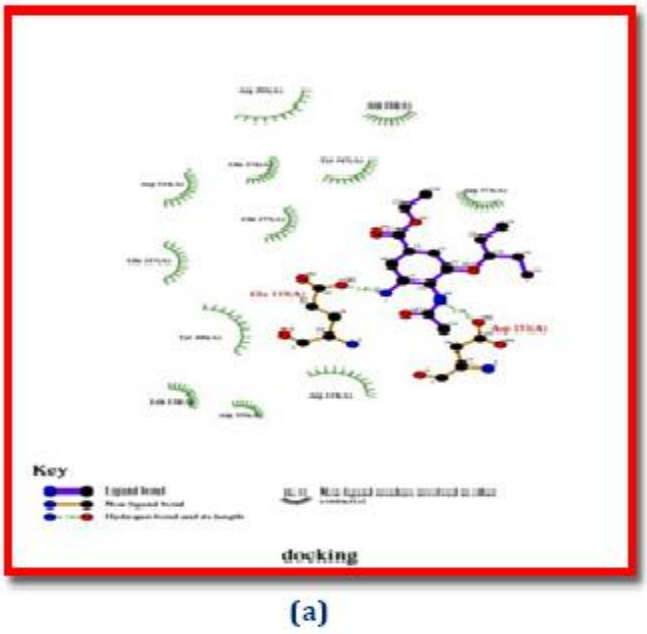

(a)

Figure 7 (a) 2D docking poses of compound Ebilfumin (protein with ligand)

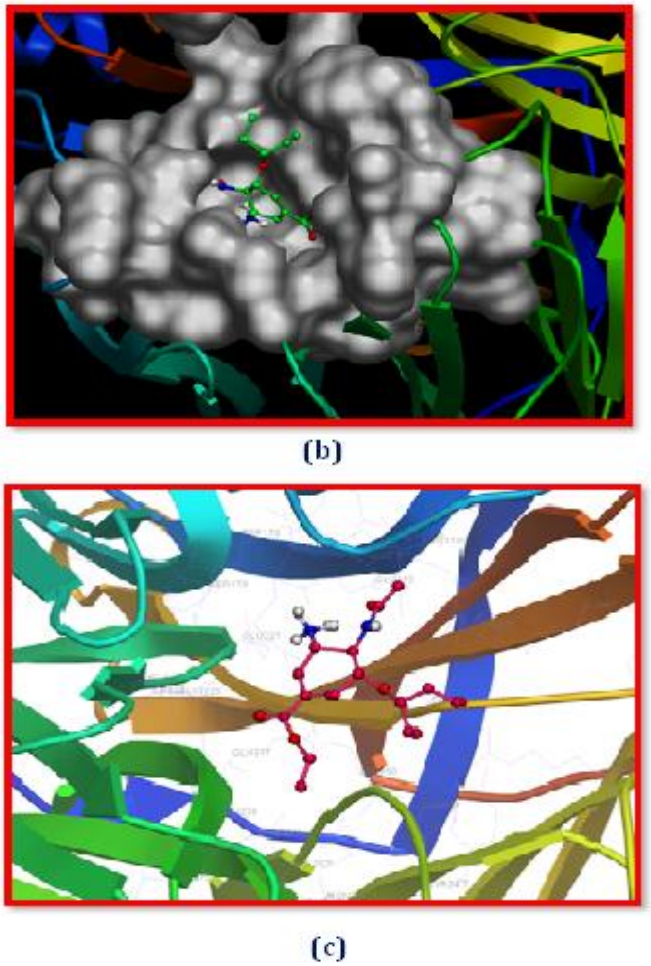

Figure 7 (b, c) 3D docking poses of compound Ebilfumin (protein with ligand)

5. CONCLUSION

The FT-IR and FT-Raman have been recorded and the detailed vibrational assignment is presented for Ebilfumin for the first time. A complete vibrational investigation of the title compound has been performed using FT-IR and Raman spectroscopic techniques and the various modes of vibrations were analysis. The equilibrium geometries, infrared intensities and Raman scattering activities of the molecule were determined and analyzed by B3LYP with 6-31G(d,p) basis sets. The simulated FT-IR and Raman spectra of the title compound show good agreement with the observed spectra. The stability and intramolecular interactions have been interpreted by NBO analysis and the transactions give stabilization to the structure have been identified by second order perturbation energy calculations. The natural atomic charges of the title molecule have been studied by DFT methods. Absorption maxima (λ_{max}) of title molecules was calculated by TD-DFT method and compared with the experimental UV–Visible spectra. HOMO and LUMO orbitals have been visualized. It has been conclude that the lowest singlet excited state of the title molecule is mainly derived from the HOMO-LUMO electron transition. The MESP map shows the negative potential sites are on oxygen and nitrogen atoms as well as the positive potential sites are around the hydrogen atoms. The molecular docking of the compound shows the various interactions between the ligand and protein active respectively.

REFERENCES

[1]. Fleming DM, ElliotAJ, 2005. A winter's tale: Comingtoterms with winter respiratory illnesses. London: Health Protection Agency.

[2]. Weber O, 2009. The role of viruses in the etiology and pathogenesis of common cold. In: Eccles RWO, editor. Common Cold. Basel, Switzerland: Birkhauser Verlag. 132–133.

[3]. Call S A, Vollenweider MA, (2005). Does this patient has influenza, JAMA. 293, 987–997.

[4]. Nicholson KG, 1992. Clinical features of influenza. Semin Respir Infect. 7, 26–37.

[5]. Monto AS, Gravenstein S, 2000. Clinical signs and symptoms predicting influenza infection. Arch. Intern. Med, 160, 3243–3247.

[6]. Boivin G, Hardy I, 2000. Predicting influenza infections during epidemics with use of a clinical cased definition. Clin. Infect. Dis. 31, 1166–1169.

[7]. Guarner J, Paddock CD, Shieh WH 2006. Histopathologic and immunohisto-chemical features of fatal influenza virus infection in children during the 2003-2004 season. Clin Infect. Dis. 43, 132–140.

[8]. Studahl M, 2003. Influenza virus and CNS manifestations. J. Clin. Virol. 28, 225–232.

[9]. Jaimovich DG, Kumar A, Shabino CL, Formoli R, 1992. Influenza B virus infections associated with non-bacterial septic shock-like illness. J. Infect. 25, 311–315.

[10]. Cate TR, 1987. Clinical manifestations and consequences of influenza. Am. J. Medicine. 82, 15–19.

[11]. Reichert TA, Simonsen L, Sharma A, 2004. Influenza and the winter increase in mortality in the United States, 1959-1999. Am. J. Epidemiol. 160, 492–502.

[12]. Nicholson KG, Kent J, Hammersley V, Cancio E, 1996. Risk factors for lower respiratory complications of rhinovirus infections in elderly people living in the community: prospective cohort study. BMJ. 313, 1119–1123.

[13]. Treanor JJ, Hayden FG, Vrooman PS, 2000. Efficacy and safety of the oral neuraminidase inhibitor oseltamivir in treating acute influenza: a randomized controlled trial. US oral Neuraminidase Study Group. JAMA. 283, 1016–1024.

[14]. Aoki FY, Macleod MD, Paggiaro P, 2003. IMPACT Study Group. Early administration of oral oseltamivir increases the benefits of influenza treat- ment. J. Antimicrob Chemother. 51, 123–129.

[15]. Whitley RJ, Boucher CA, Lina B, 2013. Global assessment of resistance to neuraminidase inhibitors, 2008-2011: the Influenza Resistance Information Study (IRIS). Clin. Infect. Dis. 56, 1197–1205.

[16]. Jefferson T, Jones MA, Doshi P, 2014. Neuraminidase inhibitors for preventing and treating influenza in healthy adults and children. Cochrane Database Syst. Rev. 4:CD008965.

[17]. Gaussian Inc., Gaussian 03 Program, Gaussian Inc., Wallingford, 2004.

[18]. Schlegel. H.B, 1982. Optimization of equilibrium geometries and transition structures, J. Comput. Chem. 3, 214–218.

[19]. Frisch A., Nielson A.B., Holder A.J. Gaussview User Manual, Gaussian Inc., Pittsburgh, PA, 2000.

[20]. Jamróz M.H., 2004. Vibrational Energy Distribution Analysis. VEDA 4, Warsaw.

[21]. Handy N.C., Maslen P.E., Amos R.D., 1993. Study of methane, acetylene, ethene, and benzene using Kohn-Sham theory, J. Phys. Chem. 97, 4392–4396.

[22]. Krishnakumar V., Mathammal R., Muthunatesan S., 2008. FT-IR and Raman spectra vibrational assignments and density functional calculations of 1-naphthyl acetic acid. Spectrochim. Acta 70A , 210–216.

[23]. Glendening E.D., Reed A.E., Carpenter J.E., Weinhold F., 1998. NBO Version3.1, TCI, University of Wisconsin, Madison.

[24]. Sutton. L. E., 1958. Tables of Interatomic Distances, Chemical Society. London.

[25]. Govindarasu, K. Kavitha, E, (2014). Vibrational spectra, molecular structure, NBO, NMR, UV, first order hyperpolarizability, analysis of (S)-(−)-N-(5-Nitro-2-pyridyl) alaninol by Density functional theory. Spectrochim. Acta A 127, 498–510.

[26]. Sartori, A., Dell'amico, L., Battistini, L., 2014. Synthesis, structure and inhibitory activity of a stereoisomer of oseltamivir carboxylate. Org.Biomol.Chem. 12, 1561-1569.

[27]. Sanner, M.F. 1999. Python: a programming language for software integration and development. Journal of Molecular Graphics and Modelling. 17, 57–61.

[28]. Adeniyi, A.A. Ajibade, P.A. 2012. Inhibitory activities and possible anticancer targets of Ru(II)-based complexes using computational docking method. Journal of Molecular Graphics and Modelling. 38, 60–69.

[29]. Rene Thomsen and Mikael H. Christensen, 2012. MolDock: A New Technique for High-Accuracy Molecular Docking. J. Med. Chem., 55, 623-638.

[30]. National Institute of Standards and Technology. Vibrational Frequency Scaling Factors (accessed 24.09.2007).

[31]. Andersen,N. H., Nielsen, C. J. , Klaeboe, P. , Guirgis, G. A. Overby J. S. Askarian, S. M. 2014. Infrared and Raman spectra, DFT-calculations and spectral assignments of 1,3,5-trisilacyclohexane. J. Mol. Struct. 1076, 419–425.

[32]. Guirgis, G. A. Dukes, H. W. Wyatt, J. K. Nielsen, C. J. Horn, A. Aleksa, V. Klaeboe, P. 2015. Vibrational spectra, quantum chemical calculations and spectral assignments of 1,1-difluoro-1-silacyclohexane. Spectrochim. Acta A 136, 51–57.

[33]. Varsanyi, G. 1973. Assignments for Vibrational Spectra of Seven Hundred Benzene Derivatives. Academic Kiaclo, Budapet.

[34]. Govindarajan, M. Periyandy, S. Carthigayen, K. 2012. FT-IR and FT-Raman spectra, thermo dynamical behavior, HOMO and LUMO, UV, NLO properties, computed frequency estimation analysis and electronic structure calculations on α-bromotoluene. Spectrochim. Acta 97, 411–422.

[35]. Colthup, N.B. Daly, L.H. Wiberley, S.E. 1990. Introduction to Infrared and Raman Spectroscopy, Academic Press, New York.

[36]. Meier, R.J. Maple, J.R. Hwang, M.J. Hagler, A.T. 1995. Molecular modeling urea-and melamine-formaldehyde resins. 1. a force field for urea and melamine, J. Phys. Chem. 99, 5445–5456.

[37]. Sajan, D. Binoy, J. Pradeep, B. Krishnan, K. V. Kartha, V. B. Joe, I. H. Jayakumar, V. S, 2004. NIR-FT Raman and infrared spectra and ab initio computations of glycinium oxalate. Spectrochim. Acta A60, 173.

[38]. Krishnakumar, V. Balachandran, V. Chithambarathanu, T. 2005. Density functional theory study of the FT-IR spectra of phthalimide and N-bromophthalimide. Spectro.chim. Acta A, 62, 918–925.
[39]. Puviarasan, N. Arjunan, V. Mohan, S. Turk. 2002. Vibrational spectroscopic, UV-Vis, molecular structure and NBO analysis of Rabeprazole. J. Chem. 26, 323–334.
[40]. Varsanyi, G. 1969. Vibrational Spectra of Benzene Derivatives, Academic Press, New York.
[41]. Krishnakumar, V. John Xavier, R. 2003. Norma l coordinates analysis of 2-mercapto and 4, 6-dihydroxy-2-mercapto pyrimidines. Indian J. Pure Appl. Phys. 41, 597–602.
[42]. Krishnakumar, V. Prabavathi, V.N. 2008. Quantum mechanical study of the structure and spectroscopic (FT-IR, FT-Raman, 13C, 1H and UV), NBO and HOMO-LUMO analysis of 2-quinoxaline carboxylic acid. Spectrochim. Acta A 71, 449–457.
[43]. Altun, A. Golcuk, K. Kumru, M, 2003. Structure and vibrational spectra of p-methylaniline: Hartree-Fock, MP2 and density functional theory studies. J. Mol. Struct. 637, 155–169.
[44]. Fleming, I. 1976. Frontier Orbitals and Organic Chemical Reactions, Wiley, London.
[45]. Lewis, F.V. Ioannides, C. Parke, D.V. 1997. Molecular modelling of CYP2E1 enzymes from rat, mouse and man: An explanation for species differences in butadiene metabolism and potential carcinogenicity, and rationalization of CYP2E substrate specificity. Xenobiotica 118, 93–113.
[46]. Govindarasu, K. Kavitha, E. 2014. Synthesis, structural, spectral (FT-IR, FT-Raman, UV, NMR), NBO and first order hyperpolarizability analysis of N-phenylbenzenesulfonamide by density functional theory. Spectrochim. Acta A 133, 417–431.
[47]. Murray, J.S. Sen, K. 1996. Molecular Electrostatic Potential Concepts and Applications, Elsevier Science. B.V, Amsterdam, the Netherlands.